PAPER • OPEN ACCESS

Evolution mechanism of principal modes in climate dynamics

To cite this article: Yongwen Zhang *et al* 2020 *New J. Phys.* **22** 093077

View the article online for updates and enhancements.

New Journal of Physics
The open access journal at the forefront of physics

PAPER

CrossMark

Evolution mechanism of principal modes in climate dynamics

Yongwen Zhang[1,2,3] (iD), Jingfang Fan[4,5] (iD), Xiaoteng Li[6], Wenqi Liu[1] and Xiaosong Chen[4,*] (iD)

1 Data Science Research Center, Kunming University of Science and Technology, Kunming 650500, Yunnan, People's Republic of China
2 Department of Physics, Bar-Ilan University, Ramat Gan 52900, Israel
3 Department of Solar Energy and Environmental Physics, The Jacob Blaustein Institutes for Desert Research, Ben-Gurion University of the Negev, Midreshet Ben-Gurion 84990, Israel
4 School of Systems Science, Beijing Normal University, Beijing 100875, People's Republic of China
5 Potsdam Institute for Climate Impact Research, 14412 Potsdam, Germany
6 Harvest Fund Management Co., Ltd, 100005 Beijing, People's Republic of China
* Author to whom any correspondence should be addressed.

E-mail: zhangyongwen77@gmail.com and chenxs@bnu.edu.cn

Abstract

Eigen analysis has been a powerful tool to distinguish multiple processes into different simple principal modes in complex systems. For a non-equilibrium system, the principal modes corresponding to the non-equilibrium processes are usually evolving with time. Here, we apply the eigen analysis into the complex climate systems. In particular, based on the daily surface air temperature in the tropics (30° S–30° N, 0° E–360° E) between 1979-01-01 and 2016-12-31, we uncover that the strength of two dominated intra-annual principal modes represented by the eigenvalues significantly changes with the El Niño/southern oscillation from year to year. Specifically, according to the 'regional correlation' introduced for the first intra-annual principal mode, we find that a sharp positive peak of the correlation between the El Niño region and the northern (southern) hemisphere usually signals the beginning (end) of the El Niño. We discuss the underlying physical mechanism and suppose that the evolution of the first intra-annual principal mode is related to the meridional circulations; the evolution of the second intra-annual principal mode responds positively to the Walker circulation. Our framework presented here not only facilitates the understanding of climate systems but also can potentially be used to study the dynamical evolution of other natural or engineering complex systems.

1. Introduction

Complexities of climate systems are generally due to the existence of multi-scale phenomena with a wide variety of space and time scales [1]. Small-scale phenomena such as convection and precipitation [2] are driven by large-scale forces such as the extratropical cyclones, planetary-scale waves, and meridional circulations. The El Niño/southern oscillation (ENSO) is one of the most important phenomena in this planet, referring to vary between anomalously warm (El Niño) and cold (La Niña) phases in the eastern Pacific, which can cause the global impacts on year-to-year time scales [3, 4].

In 1969, Bjerknes postulated that the Bjerknes feedback (the Walker circulation) was essential to the mechanism of the ENSO [5]. Still, the mechanism has not been fully understood [6]. The alternations between warm and cold phases are quite irregular in the El Niño basin [7]. There is a controversy over whether the ENSO is controlled by stochastic processes [8]. Heat frequently exchanges between the ocean and atmosphere near the equator. Moreover, the energy is transported over a great distance from the equator to the polar regions by the general circulations [9, 10]. From the physics point of view, the ENSO could be triggered by small-scale and short-term processes, if the critical condition (long-range correlation or teleconnection) is satisfied in this system [11–13]. Although the ENSO has known as an inter-annual phenomenon, it was found to be coupling with intra-annual processes [14–17], even with the higher frequency processes [18, 19]. A significant intra-annual variation of the ENSO has been observed–El Niño

events tend to peak in boreal winter and fall rapidly in boreal spring [20, 21]. Some studies [22–24] showed that the ENSO combines with an annual cycle.

Eigen analysis has been a classic technique to distinguish multiple physical processes into a combination of some single processes and capture the individual feature. It is widely used in community detection, image recognition and empirical data analysis [25–27]. Also, it has emerged as a very popular tool in climate science called as the empirical orthogonal function (EOF) analysis [28] and been used to search for the features of the ENSO [29–31]. The inter-annual principal modes associated with the ENSO have been found based on the EOF analysis [22, 29]. Due to the multi-scale characteristics of climate in time and space, the interdisciplinary complex-based approaches such as complex networks [32–37] and wavelet analysis [38, 39] have been proved to be very powerful tools to study climate phenomena. Some recent studies have applied these complex-based methods to enhance the prediction skill of the El Niño [40–42] and study its impacts [43, 44]. Actually, the essential of climate networks is the correlation matrix as well as the eigen analysis [45, 46]. Fast fluctuations of the correlations observed during El Niño periods cause the links to break in the climate networks [47, 48].

Here, we use eigen analysis to study the intra-annual principal modes of daily surface air temperature (SAT). Previous studies mentioned above focused on the inter-annual principal modes for the deseasonalized data. However, the preprocess of removing seasonality could artificially change the annual cycles. Thus, we use the raw SAT data here in comparison to use the deseasonalized data. Furthermore, it is different with previous studies that we focus on the intra-annual principal modes for the correlation matrix in a 365 days' window and their temporal evolution with the time window. Previous EOF analyses assume that the eigenvalues and eigenvectors remain constant from year to year. Here, the intra-annual principal modes can change with time in the non-equilibrium system. These changes can be identified by fluctuations of the eigenvalues and eigenvectors. The eigenvalue plays an important role to describe the macroscopic properties of physical systems, which is related to the susceptibility of systems [49, 50]. The detailed spatial patterns are performed by the distributions of eigenvectors. This paper is organized as follows. Section 2 describes the materials and methods. In section 3 we present the results, and provide the conclusions in section 4.

2. Materials and methods

2.1. Data
The used raw data are daily SAT at 2 m and surface wind at 10 m provided by the European center for medium-range weather forecasts interim reanalysis (ERA-Interim) [51] on a $2.5° \times 2.5°$ latitude–longitude grid over the tropics region ($30°$ S–$30°$ N,$0°$ E–$360°$ E), resulting in $25 \times 144 = 3600$ grids. The dataset spans the period between 1979-01-01 and 2016-12-31. El Niño or La Niña events are defined when the oceanic Niño index (ONI) exceeds $\pm 0.5°$C for a period of five months or more. The ONI is defined as the 3 month running mean of ERSST.v5 SST anomalies in the El Niño 3.4 region ($5°$ S–$5°$ N, $190°$ E–$240°$ E). To obtain the deseasonalized data, we subtract from each day's temperature the yearly mean temperature of that day. Specifically, if we take the raw daily SAT time series of a given grid to be $S^y(t)$, where y is year and t is the day in a range from 1 to 365; the deseasonalized time series $S'^y(t) = S^y(t) - \frac{1}{N_y}\sum_y S^y(t)$, where N_y is the total number of years from 1979 to 2016.

2.2. Methodology
2.2.1. Principal modes of temperature fluctuation
In a climate system consisting of N grids, the temperature of a grid i at time t within a time window of length d is defined as $S_i(t; T)$, where T represents the central time of the time window. The average temperature of grid i for the time window is calculated as

$$\bar{S}_i^T = \frac{1}{d}\sum_{t=1}^{d} S_i(t; T). \tag{1}$$

At the time t, the grid i has a temperature fluctuation $\delta S_i(t; T) = S_i(t; T) - \bar{S}_i^T$. The standard deviations of temperature for land and sea are very different. Thus we consider here the normalized fluctuation $\delta \hat{S}_i(t; T) = \delta S_i(t; T)/\sqrt{\langle [\delta S_i(t; T)]^2 \rangle}$. The correlation of temperature for the time window T between grids i and j is defined as

$$C_{ij}(T) = \left\langle \delta \hat{S}_i(t; T) \cdot \delta \hat{S}_j(t; T) \right\rangle, \tag{2}$$

which is the Pearson correlation coefficient. Using $C_{ij}(T)$ as its elements, we obtain then an $N \times N$ correlation matrix $C(T)$ with N eigenvectors and eigenvalues. The eigenvector corresponding to eigenvalue $\lambda_n(T)$ is $b_n(T)$ which satisfies the equation

$$C(T) \cdot b_n(T) = \lambda_n(T)b_n(T), \quad n = 1, 2, \ldots, N. \tag{3}$$

The eigenvalues are numbered in the order $\lambda_1(T) \geqslant \lambda_2(T), \ldots, \geqslant \lambda_N(T) \geqslant 0$. The summation of all the eigenvalues satisfies $\sum_n \lambda_n = N$.

The eigenvectors follow the condition

$$b_n(T) \cdot b_l(T) = \sum_i b_{in}(T)b_{il}(T) = \delta_{nl}, \tag{4}$$

where $\delta_{nl} = 1$ at $n = l$ and $\delta_{nl} = 0$ otherwise. All eigenvectors are normalized and orthogonal to each other.

Using the nth eigenvector $b_n(T)$, the nth principal mode can be obtained as

$$a_n(t; T) = \sum_{i=1}^{N} b_{in}(T)\delta\hat{S}_i(t; T). \tag{5}$$

The correlation between principal modes $a_n(T)$ and $a_l(T)$ is

$$\langle a_n(T) \cdot a_l(T) \rangle = \frac{1}{d}\sum_{t=1}^{d} a_n(t; T)a_l(t; T) = \lambda_n(T)\delta_{nl}. \tag{6}$$

So different principal modes are independent for a certain T. The square amplitude of a principal mode is equal to the corresponding eigenvalue. Furthermore, we can shift the time T to obtain the evolution of eigenvalues and eigenvectors.

2.2.2. Regional correlation in principal modes

By equation (5), $\delta\hat{S}_i(t; T)$ can be considered as the summation of contributions from all principal modes

$$\delta\hat{S}_i(t; T) = \sum_{n=1}^{N} b_{in}(T)a_n(t; T). \tag{7}$$

Combining equations (7) and (6) into (2), the correlation between girds i and j can be written as

$$C_{ij}(T) = \sum_{n=1}^{N} b_{in}(T)b_{jn}(T)\lambda_n(T). \tag{8}$$

To quantify the correlation of the nth principal mode between region A (such as the El Niño 3.4 region) and region B (such as the northern or southern hemisphere), the 'regional correlation' is defined as

$$C_{AB}^n(T) = \frac{\sum_{i\in A}\sum_{j\in B}\Theta_{in}(T)b_{in}(T)\Theta_{jn}(T)b_{jn}(T)\lambda_n(T)}{N_A \times N_B}, \tag{9}$$

where N_A and N_B are total numbers of girds within region A and B respectively. To exclude noises of b_{in}, we define $\Theta_{in}(T) = 1$ for $|b_{in}(T)| > \Delta$ and $\Theta_{in}(T) = 0$ otherwise. The average value of b_{in} is $\frac{1}{\sqrt{N}}$ and we choose a threshold $\Delta = \frac{1}{2}\frac{1}{\sqrt{N}} = 0.008$. The regional correlation C_{AB}^n reflects the relations between two specific regions, which is resulted by the nth principal mode. It also changes with the time T.

3. Results

We start to obtain the deseasonalized data as described in section 2.1. Since the seasonal cycle is 365 days, we take the length of time window $d = 365$. For a time window with its center in the month T, we can obtain the correlation matrix $C(T)$ and do eigen-decomposition. With T shifted by one month each time, their evolution with the time window can be obtained for both the raw and deseasonalized data.

We calculate the intra-annual principal mode $a_n(T)$ by equation (5). For example, figure 1(a), (c) show the principal modes $a_1(t; T)$ and $a_2(t; T)$ of the raw data with respect t at different T corresponding to a normal time (1994.01), an El Niño time (1998.01), and a La Niña time (2000.01) respectively. A dominant annual cycle in the first principal mode $a_1(t; T)$ is observed in figure 1(a). The mode $a_1(t; T)$ decreases as t from February to August, and increases from August to the next February. The second principal mode $a_2(t; T)$ is presented in figure 1(c), where an annual cycle is also observed. In comparison with figure 1(a),
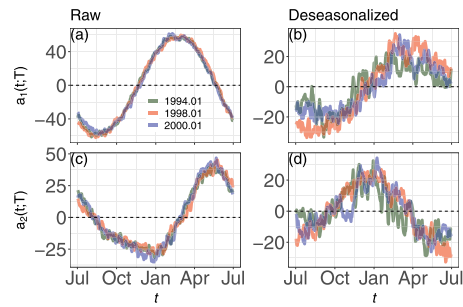
Figure 1. The first principal mode for (a) the raw data and (b) the deseasonalized data for different T: 1994.01, 1998.01 and 2000.01. (c), (d) Same as (a), (b) but for the second principal mode.
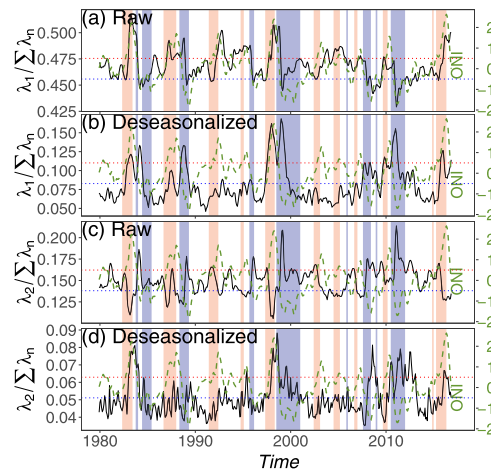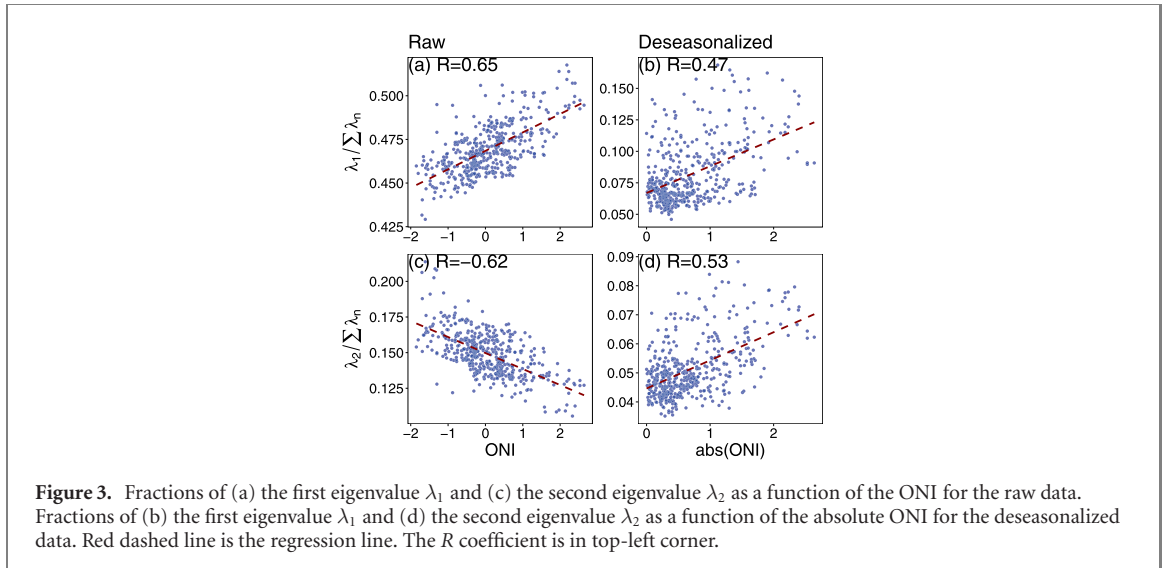

Figure 2. Fractions of the first eigenvalue λ_1 as a function of time T (black solid line, left scale) for (a) the raw data and (b) the deseasonalized data. (c), (d) Same as (a), (b) but for the second eigenvalue λ_2. Green dashed line is the ONI (right scale). Red and blue shades represent respectively El Niño and La Niña periods.

the annual cycle of $a_2(t; T)$ has a shift. It is reasonable that the annual cycle plays the dominant role in $a_1(t; T)$ for the raw data, since the influences of Sun are the deciding factors to result in the seasonal fluctuations of surface air temperature. For $a_2(t; T)$ of the raw data, figure 5(a) shows that the eastern Pacific is a prominent area whose seasonal cycle has been found to follow the southern hemisphere but it is shifted by a few months [52]. Thus, the annual cycle also domains in the second principal mode. Besides, we apply the spectrum analysis to the principal modes and find that the period 365 days is dominated for all the cases in figure 1 and their phases are similar for different years. The results indicate that the intra-annual principle modes of the deseasonalized data still exit a common annual cycle for different years (see figures 1(b) and (d)).

To further quantify differences of the intra-annual principal modes in different time T, we calculate the variances of the principle modes which are the eigenvalues (see equation (6)). The eigenvalues can represent the strength of principal modes. The fractions of the first eigenvalues and the second eigenvalues with T from 1979.06 to 2016.06 are shown in figures 2(a) and (c) for the raw data. The fraction $\lambda_1(T)/\sum_n \lambda_n(T)$ is more than 40%. The fraction of the second eigenvalue varies from 10% to 20%. For the deseasonalized data in figure 2(b) and (d), the fractions of the corresponding eigenvalues are smaller than those of the raw data, since temperature fluctuations are smaller in the deseasonalized data. The results show that the evolution of eigenvalues significantly changes with time for both the raw and deseasonalized data. For instance, the peaks of $\lambda_1(T)/\sum_n \lambda_n(T)$ for the raw data correspond to EI Niño events and its valleys correspond to La Niña events in figure 2(a). $\lambda_2(T)/\sum_n \lambda_n(T)$ in figure 2(c) is opposite to $\lambda_1(T)/\sum_n \lambda_n(T)$ in figure 2(a). For the deseasonalized data, it seems that both EI Niño and La Niña correspond to the peaks of eigenvalues in figures 2(b) and (d). Thus, the eigenvalues mainly describe the strength of intra-annual principal modes of temperature in response to the ENSO force.

We show that the fractions of the first and second eigenvalues as a function of the ONI in figure 3. Figure 3(a) and (c) show that both the first and second eigenvalues for the raw data have a strong relevance to the ONI. The R coefficient between the fraction of λ_1 and the ONI is characterized by their Pearson

Figure 3. Fractions of (a) the first eigenvalue λ_1 and (c) the second eigenvalue λ_2 as a function of the ONI for the raw data. Fractions of (b) the first eigenvalue λ_1 and (d) the second eigenvalue λ_2 as a function of the absolute ONI for the deseasonalized data. Red dashed line is the regression line. The R coefficient is in top-left corner.
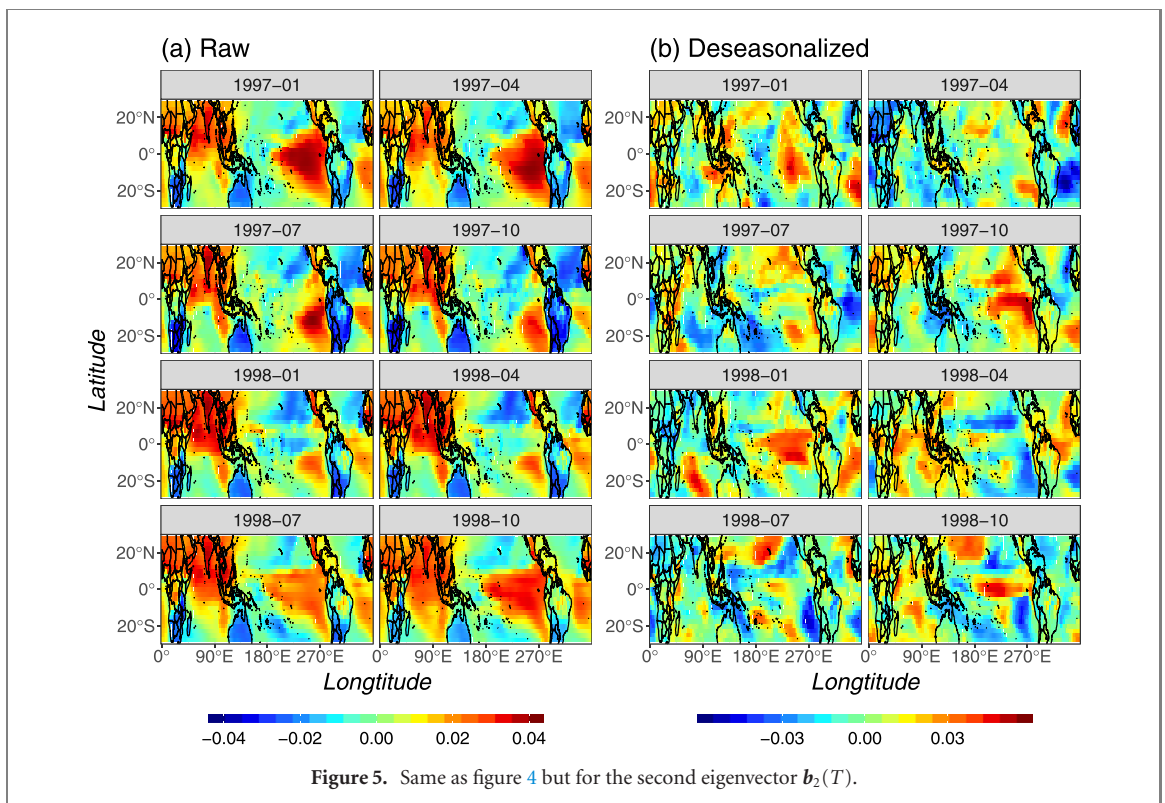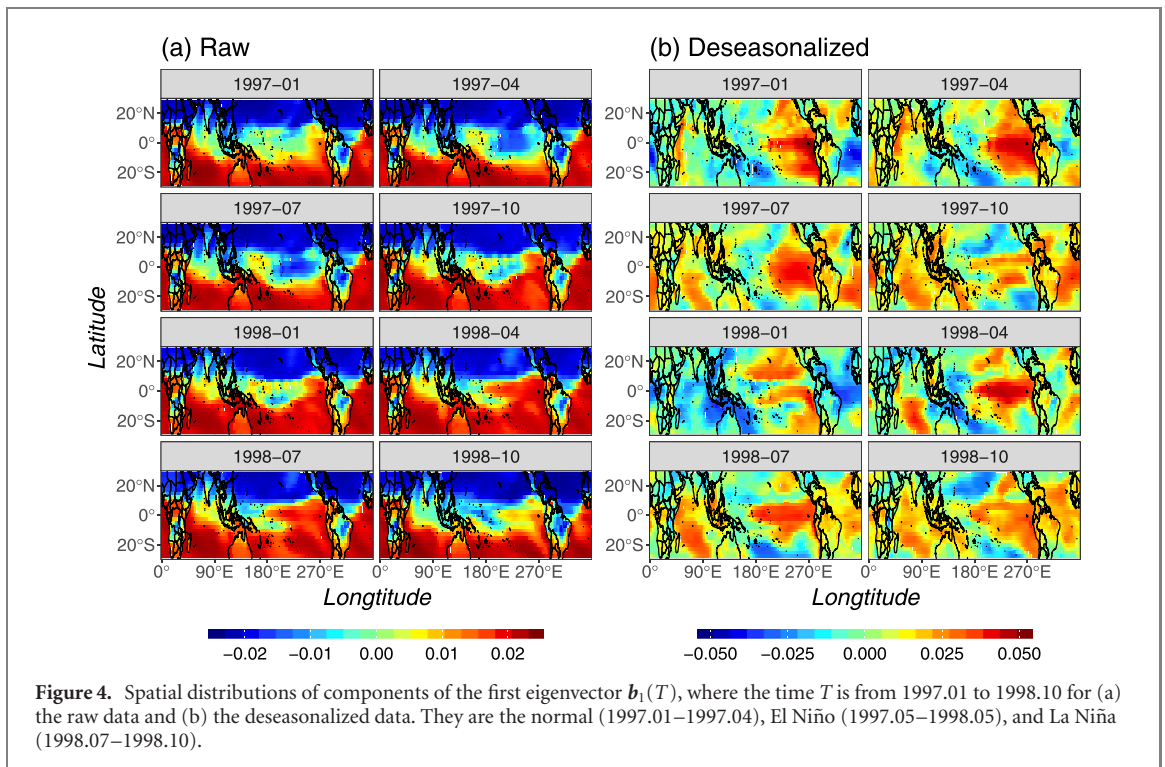
correlation coefficient, which is equal to 0.65 in figure 3(a). The R coefficient between the fraction of λ_2 and the ONI is equal to -0.62 in figure 3(c). Moreover, the R coefficient between the fractions of λ_1 and λ_2 is equal to -0.75. This indicates that the first (second) principal mode is reinforced (weakened) during El Niño periods. We also compare with the results of the deseasonalized data as shown in figure 3(b) and (d). Since their relations are nonlinear with the ONI, we use the absolute ONI here. The R coefficients for the deseasonalized data (see figure 3(b) and (d)) are positive and smaller than the absolute R coefficients of the raw data. The results indicate the better correlations for the raw data than the deseasonalized data. We also test other smaller eigenvalues such as the third and fourth eigenvalues. They do not show a significant correlation with the ONI or its absolute value.

To understand spatial features of intra-annual principle modes, we study the spatial distribution of $\boldsymbol{b}_n(T)$. An example is depicted in figure 4 for T from 1997.01 to 1998.10, which spans the strong 1997−98 El Niño event. In the Jan of 1997, the ONI was -0.49 and increased to 0.74 in the May of 1997, which demonstrate the emergence of an El Niño event. This event lasted until to the Aug of 1998. With the further decrease of the ONI, a La Niña event appeared in the July of 1998 and lasted until 2001. The distributions of b_{i1} are divided mainly into two large clusters for the raw data in figure 4(a). One is in the northern hemisphere and has negative components. Another one is in the southern hemispheres and has positive components. In addition, there are two small clusters with negative components and located in the rainforests of Congo (Africa) and Amazon (South America). The components of the interface between two large clusters are nearly zero. The interface exists around the equator and varies greatly with time T.

In the normal phase at the beginning, the El Niño 3.4 region (5° S−5° N, 190° E−240° E) belongs to the interface and the corresponding $b_{i1}(T)$ are nearly zero (see figure 4(a) for 1997.01). The temperature fluctuations in the region are nearly independent of the first principal mode. Later, the components $b_{i1}(T)$ in a part of the region become negative. The temperature fluctuations there are dominated by the first principal mode $\delta \hat{S}_i(t; T) \sim b_{i1}(T) a_1(t; T)$. The negative components (blue) in the El Niño 3.4 region (see figure 4(a) for 1997.04 and 1997.07) result in the temperature fluctuations increases as $a_1(t; T)$ decreases from February to August (see figure 1(a)) in comparison with the normal phase. Then an El Niño appeared, and the components in the El Niño region gradually change from negative to positive. We can see that the components $b_{i1}(T)$ in a part of the El Niño region become positive later (see figure 4(a) for 1998.04 and 1998.07). These positive components (red) can contribute the decrease of temperature and end the El Niño to the La Niña after next February. For the deseaonalized data in figure 4(b), the strong components mainly distribute in the eastern Pacific which are consistent with the distribution of temperature anomalies. Moreover, the components change with time T over the entire region.

The spatial distributions of $\boldsymbol{b}_2(T)$ are shown in figure 5. For the second eigenvector of the raw data in figure 5(a), there are two large clusters with positive components in the Indian ocean and the eastern Pacific and their temperature fluctuations are coupled. At the beginning of 1997 (see figure 5(a) for 1997.01 and 1997.04), there is a large cluster with positive components in the eastern Pacific. With the emergence of El Niño from 1997.07 to 1998.04 in figure 5(a), this cluster becomes smaller and weaker. Even a cluster with negative components appears in the region. After the end of El Niño, there is a La Niña and a cluster with positive components appears again in the eastern Pacific (see figure 5(a) for 1998.07 and 1998.10). For the deseaonalized data, the sizes of clusters in figure 5(b) are smaller than the clusters in figure 5(a). It is

Figure 4. Spatial distributions of components of the first eigenvector $\boldsymbol{b}_1(T)$, where the time T is from 1997.01 to 1998.10 for (a) the raw data and (b) the deseasonalized data. They are the normal (1997.01–1997.04), El Niño (1997.05–1998.05), and La Niña (1998.07–1998.10).

**Figure 5.** Same as figure 4 but for the second eigenvector $\boldsymbol{b}_2(T)$.

difficult to find a regular pattern for the deseaonalized data. Thus the spatial distributions of the eigenvectors for the raw data show a better relationship with the 1997–98 El Niño event than the deseaonalized data as well as the eigenvalues.

To analyze the relationship between the ENSO and the spatial distributions of $\boldsymbol{b}_n$ for the raw data comprehensively, we calculate the regional correlation via equation (9) from 1979 to 2016. The regional correlation of the first principal mode for the raw data between the El Niño 3.4 region and the northern region (5° N–30° N, 0° E–360° E) can be obtained as C_{EN}^1. Similarly we obtain the regional correlation C_{ES}^1 between the El Niño 3.4 region and the southern region (5° S–30° S, 0° E–360° E). The regional correlation
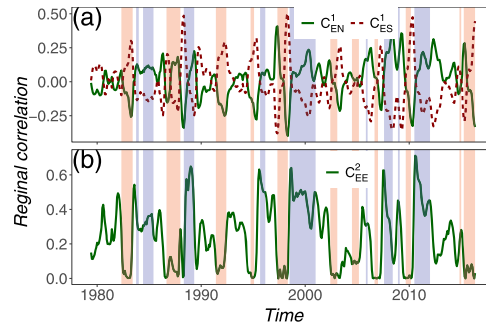
Figure 6. Regional correlation for (a) the first principal mode and (b) the second principal mode for the raw data. Red and blue shades represent respectively El Niño and La Niña periods.
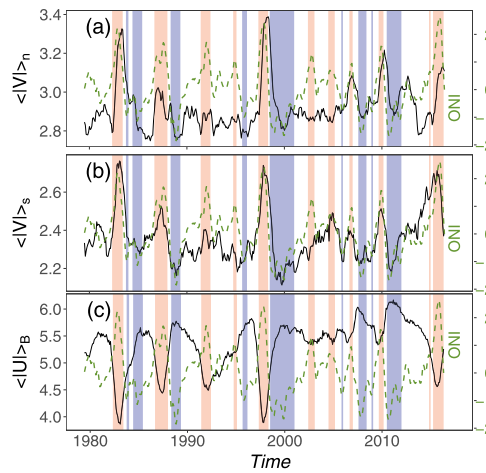
Figure 7. Mean V wind strength (a) $\langle |V| \rangle_n$ and (b) $\langle |V| \rangle_s$, and (c) mean U wind strength $\langle |U| \rangle_B$ as a function of time T (black solid line, left scale). Green dashed line is the ONI (right scale). Red and blue shades represent respectively El Niño and La Niña periods.

C_{EN}^1 (solid line) and C_{ES}^1 (dashed line) are shown as functions of time T in figure 6(a). A large C_{EN}^1 (C_{ES}^1) represents that the El Niño region is positively correlated with the north (south) region, as shown in figure 4(a). In normal phases, figure 6(a) shows that C_{EN}^1 and C_{ES}^1 are close to zero. We find that C_{EN}^1 has a peak before the emergence of (nearly 70%) El Niño events in figure 6(a). This could imply a possible early warning signal for the El Niño. Instead, C_{ES}^1 has a sharp peak at the end of (nearly 90%) El Niño events. Such correlation between the El Niño region and the northern (southern) hemisphere for the first principal mode of the raw data could be driven by the Hadley circulation [53], which is a general meridional ocean-atmospheric circulation.

The second principal mode of the raw data is dominated by the cluster components in the equatorial eastern Pacific (see figure 5(a)). Thus we calculate the regional correlation of the second principal mode for the El Niño 3.4 region itself (like autocorrelation) as C_{EE}^2. Figure 6(b) shows that C_{EE}^2 is strong during La Niña phases and becomes weak during El Niño phases. It indicates that the strength of the cluster in the El Niño region is anti-correlated with the ONI in this region. The correlation coefficient between the ONI and C_{EE}^2 is -0.76. The regional correlation C_{EE}^2 is positively related to the Walker circulation, which is a zonal ocean-atmosphere circulation in the Pacific (the east–west surface temperature contrast reinforces an east–west air pressure difference across the Pacific basin, which in turn drives trade winds). During La Niña, the Walker circulation becomes strong with the strong trade winds. During El Niño instead, the Walker circulation becomes weak with the weak trade winds [2]. Moreover, the annual cycle of $a_2(t; T)$ in figure 1(c) is also associated with the seasonal variation of the Walker circulation which is very pronounced in January [54].

We further prove our conjectures by studying the daily surface wind field (10 m) which is used to character the zonal and meridional circulations. The wind is divided into meridional part V and zonal part U. For the northern region (0°–30° N, 190° E–240° E), the average magnitude $\langle |V| \rangle_n$ is calculated and

presented in figure 7(a). We make the average for one year with its center in the month T. The average magnitude of V in the southern region $(0°-30°$ S, $190°$ E$-240°$ E) is denoted as $\langle|V|\rangle_s$. The results obtained are shown in figure 7(b). We can see that El Niño events are accompanied usually by strong $\langle|V|\rangle_{n,s}$. In general, $\langle|V|\rangle_n$ is larger than $\langle|V|\rangle_s$. This result further demonstrates that the connection between the equator and northern (southern) hemisphere becomes stronger during El Niño in agreement with the results of the regional correlation C_{EN}^1 and C_{ES}^1 in figure 6(a).

For the zonal part of wind, we calculate its average magnitude $\langle|U|\rangle_B$ in the Niño 3.4 regions. The results obtained are depicted in figure 7(c). During El Niño events, there are obvious decreases of $\langle|U|\rangle_B$ as similar as C_{EE}^2 in figure 6(b). We obtain that the correlation between C_{ES}^1 and the mean V wind strength $\langle|V|\rangle_s$ equals 0.35 (p-value $< 10^{-3}$); and the correlation between C_{EE}^2 and the mean U wind strength $\langle|U|\rangle_B$ is 0.47 (p-value $< 10^{-3}$). Both the correlation coefficients are significant. However, the wind strength $\langle|U|\rangle_B$ does not always become weak during El Niño events. It seems to show different behaviors for different El Niño, i.e., the central Pacific El Niño events such as 1994–93, 2004–05 and 2009–10 have the much stronger wind strength $\langle|U|\rangle_B$ than the eastern Pacific El Niño such as 1997–98 and 1982–83.

4. Conclusions

Here we studied the evolution of the principal modes in the climate system. Based on the daily SAT in the region $(30°$ S$-30°$ N, $0°$ E$-360°$ E) for both the raw and deseasonalized data, we found that there exist two largest intra-annual principal modes corresponding to two annual cycles within one year. The temporal evolution of the intra-annual principal modes is investigated from 1979-01-01 to 2016-12-31 by sliding the one-year time window. We showed that the eigenvalues λ_1 and λ_2 significantly response to the ENSO variability for the raw data. The Pearson correlation coefficients between the fractions of the first and the second eigenvalues and the ONI are 0.65 and -0.62, which imply that the first (second) principal mode is reinforced during El Niño (La Niña) and weakened during La Niña (El Niño).

The eigenvalues of the two intra-annual principal modes for the raw data have a stronger correlation with the ENSO than that for the deseaonalized data, as well as the spatial distributions of eigenvectors. We proposed a regional correlation to quantify the relations of temperature fluctuations between the El Niño region and other regions for the raw data. In normal phases, the regional correlation for the first principal mode is very weak and the temperature fluctuations in the El Niño region are dominated by the second principal mode. When the regional correlation of the northern hemisphere for the first principal mode becomes strong positive from February to August, the El Niño event will occur with a high probability. With the evolution of the El Niño event, the regional correlation of the southern hemisphere changes from negative to strong positive so that the temperature decreases fast after the next February. For the second principal mode, the autocorrelation of the El Niño region has middle value during the normal phase and large value during the La Niña phase, which correspond to normal and strong Walker circulation respectively. With the emergence of an El Niño event, the autocorrelation becomes small in relation to a weak Walker circulation leading.

We suggest that the evolution mechanism for the ENSO is the competition between the first and second intra-annual principal modes for the raw SAT data, which are related to the meridional and zonal circulations respectively. This is demonstrated partly by the mean meridional and zonal surface wind field (10 m). The meridional circulations could drive the seasonal footprint from the northern and southern hemispheres to the El Niño region such that the influences on the ENSO. Our method can also be used to study the dynamics of other non-equilibrium complex systems.

Acknowledgments

ORCID iDs

Yongwen Zhang ⓘ https://orcid.org/0000-0002-3240-7249
Jingfang Fan ⓘ https://orcid.org/0000-0003-1954-4641
Xiaosong Chen ⓘ https://orcid.org/0000-0001-9994-2011

References

[1] Hartmann D 1994 *Global Physical Climatology* (New York: Academic)
[2] Neelin J D 2011 *Climate Change and Climate Modeling* (Cambridge: Cambridge University Press)
[3] Mcphaden M J, Zebiak S E and Glantz M H 2006 *Science* **314** 1740
[4] Wang C, Deser C, Yu J Y, Dinezio P and Clement A 2017 *El Niño and Southern Oscillation (ENSO): A Review* (Berlin: Springer)
[5] Bjerknes J 1969 *Mon. Weather Rev.* **97** 163−72
[6] Mcphaden M J 2015 *Nat. Clim Change* **5** 791−5
[7] Timmermann A *et al* 2018 *Nature* **559** 535−45
[8] Neelin J D, Battisti D S, Hirst A C, Jin F F, Wakata Y, Yamagata T and Zebiak S E 1998 *J. Geophys. Res.* **103** 14261−90
[9] Jin F F 2000 *J. Atmos. Sci.* **54** 811−29
[10] Knox J A and Knox P N 2017 *Atmospheric/General Circulation* (New York: Wiley)
[11] Stanley H. E. and Ahlers G 1973 *Phys. Today* **26** 71−2
[12] Sornette D 2006 *Critical Phenomena in Natural Sciences: Chaos, Fractals, Selforganization and Disorder: Concepts and Tools* (Berlin: Springer)
[13] Zhang X, Hu G, Zhang Y, Li X and Chen X 2018 *Sci. China Phys. Mech.* **61** 120511
[14] Jin F F, Neelin J D and Ghil M 1994 *Science* **264** 70−2
[15] Tziperman E, Stone L, Cane M A and Jarosh H 1994 *Science* **264** 72−4
[16] Stein K, Timmermann A, Schneider N, Jin F F and Stuecker M F 2014 *J. Clim.* **27** 5285−310
[17] Stuecker M F, Jin F F and Timmermann A 2015 *Proc. Natl Acad. Sci. USA* **112** 13490−5
[18] Fedorov A V, Harper S L, Philander S G, Winter B and Wittenberg A 2003 *Bull. Am. Meteorol. Soc.* **84** 911−20
[19] Kessler W S 2002 *Geophys. Res. Lett.* **29** 40−4
[20] Stein K, Timmermann A and Schneider N 2011 *Phys. Rev. Lett.* **107** 128501
[21] Mcgregor S, Timmermann A, Schneider N, Stuecker M F and England M H 2011 *J. Clim.* **25** 5566−86
[22] Stuecker M F, Timmermann A, Jin F F, Mcgregor S and Ren H L 2013 *Nat. Geosci.* **6** 540−4
[23] Ren H-L, Zuo J, Jin F F and Stuecker M F 2016 *Clim. Dyn.* **46** 3753−65
[24] Guilyardi E, Wittenberg A, Fedorov A, Collins M, Wang C Z, Capotondi A, van Oldenborgh G J and Stockdale T 2009 *Bull. Am. Meteor. Soc.* **90** 325−40
[25] Newman M E J 2006 *Phys. Rev. E* **74** 1−19
[26] Zhang Y W, Hu G K, Chen X S, Chen W and Liu W Q 2019 *Sci. China Phys. Mech.* **62** 40511
[27] Hofmann T 2001 *Mach. Learn.* **42** 177−96
[28] Hannachi A, Jolliffe I T and Stephenson D B 2007 *Int. J. Climatol.* **27** 1119−52
[29] Zhang Y, Wallace J M and Battisti D S 1997 *J. Clim.* **10** 1004−20
[30] Kawamura R 1994 *J. Phys. Oceanogr.* **24** 707−15
[31] McGregor S, Ramesh N, Spence P, England M H, McPhaden M J and Santoso A 2013 *Geophys. Res. Lett.* **40** 749−54
[32] Tsonis A A, Swanson K L and Roebber P J 2006 *Bull. Am. Meteor. Soc.* **87** 585−96
[33] Donges J F, Zou Y, Marwan N and Kurths J 2009 *Eur. Phys. J. Spec. Top.* **174** 157−79
[34] Donges J F, Zou Y, Marwan N and Kurths J 2009 *Europhys. Lett.* **87** 48007
[35] Agarwal A, Caesar L, Marwan N, Maheswaran R, Merz B and Kurths J 2019 *Sci. Rep.* **9** 1−12
[36] Zhang Y, Fan J, Chen X, Ashkenazy Y and Havlin S 2019 *Geophys. Res. Lett.* **46** 12476−85
[37] Zhang Y, Chen D, Fan J, Havlin S and Chen X 2018 *Europhys. Lett.* **122** 58003
[38] Rathinasamy M, Agarwal A, Sivakumar B, Marwan N and Kurths J 2019 *Stoch. Environ. Res. Risk Assess.* **33** 2053−69
[39] Kurths J, Agarwal A., Shukla R, Marwan N, Rathinasamy M, Caesar L, Krishnan R and Merz B 2019 *Nonlinear Process. Geophys.* **26** 251−66
[40] Ludescher J, Gozolchiani A, Bogachev M I, Bunde A, Havlin S and Schellnhuber H J 2014 *Proc. Natl Acad. Sci. USA* **111** 201323058
[41] Meng J, Fan J, Ashkenazy Y and Havlin S 2017 *Chaos* **27** 035807
[42] Meng J, Fan J, Ludescher J, Agarwal A, Chen X, Bunde A, Kurths J and Schellnhuber H J 2020 *Proc. Natl Acad. Sci. USA* **117** 177−83
[43] Fan J, Meng J, Ashkenazy Y, Havlin S and Schellnhuber H J 2017 *Proc. Natl Acad. Sci. USA* **114** 7543−8
[44] Lu Z, Yuan N, Chen L and Gong Z 2020 *Geophys. Res. Lett.* **47** e2019GL086533
[45] Donges J F, Petrova I, Loew A, Marwan N and Kurths J 2015 *Clim. Dyn.* **45** 2407−24
[46] Wiedermann M, Radebach A, Donges J F, Kurths J and Donner R V 2016 *Geophys. Res. Lett.* **43** 7176−85
[47] Yamasaki K, Gozolchiani A and Havlin S 2008 *Phys. Rev. Lett.* **100** 228501
[48] Tsonis A A and Swanson K L 2008 *Phys. Rev. Lett.* **100** 228502
[49] Li X T and Chen X S 2016 *Commun. Theor. Phys.* **66** 355
[50] Hu G, Liu T, Liu M, Chen W and Chen X 2019 *Sci. China Phys. Mech.* **62** 990511
[51] Dee D P *et al* 2011 *Q. J. R. Meteorol. Soc.* **137** 553−97
[52] Wallace J M, Mitchell T P and Deser C 1989 *J. Clim.* **2** 1492−9
[53] Oort A H and Yienger J J 1996 *J. Clim.* **9** 2751−67
[54] North G R, Zhang F and Pyle J 2014 *Encyclopedia of Atmospheric Sciences* 2nd edn (Amsterdam: Elsevier)